Journal of Power Sources 271 (2014) 42–47

Contents lists available at ScienceDirect

Journal of Power Sources

journal homepage: www.elsevier.com/locate/jpowsour

Electrochemical performance of laser micro-structured nickel oxyhydroxide cathodes

Alex R. Neale [a], Yang Jin [b], Jinglei Ouyang [b], Stephen Hughes [a], David Hesp [c], Vinod Dhanak [c], Geoff Dearden [b], Stuart Edwardson [b, *], Laurence J. Hardwick [a, *]

[a] Stephenson Institute for Renewable Energy, Department of Chemistry, The University of Liverpool, Crown Street, Liverpool L69 7ZD, UK
[b] School of Engineering, The University of Liverpool, The Quadrangle, Brownlow Hill, Liverpool L69 3GH, UK
[c] Stephenson Institute for Renewable Energy, Department of Physics, The University of Liverpool, Crown Street, Liverpool L69 7ZD, UK

HIGHLIGHTS

- The surface of Ni foils was processed by ultra-short pulse length, low energy laser light.
- The technique produced periodic ripple micro-structures (LIPPS) at the surface of the Ni.
- LIPPS yields an increased electrochemical activity relative to unprocessed planar Ni by a factor of 2.5.
- LIPPS electrode modification could be relevant for Ni based micro-battery systems.

GRAPHICAL ABSTRACT

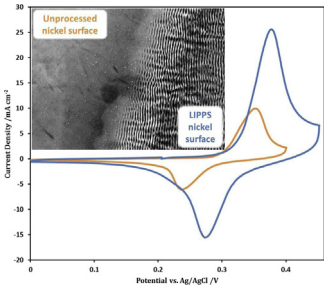

ARTICLE INFO

Article history:
Received 30 April 2014
Received in revised form
1 July 2014
Accepted 25 July 2014
Available online 4 August 2014

Keywords:
Nickel oxyhydroxide cathodes
Laser-induced periodic plasmonic structures
Micro-batteries
Nickel oxide

ABSTRACT

This study describes the preparation and analysis of laser micro-structured nickel metal electrodes for application as a cathode material in micro-batteries based on the nickel oxyhydroxide chemistry. Using ultra-short pulse length lasers (picoseconds to femtoseconds); surface micro-structures in the form of ripples are rapidly generated at the surface of nickel metal cathodes. These ripple micro-structures, with a periodic spacing approximately equal to the wavelength of laser radiation used, are more commonly referred to as laser-induced periodic plasmonic structures (LIPPS). The electrochemical activity of the LIPPS nickel metal cathodes is investigated in aqueous KOH using cyclic voltammetry. Across a wide range of scan rates, the results of the voltammetry show that the formation of LIPPS yields a considerable enhancement in the electrochemical activity of the nickel surface. The observed enhancement is attributed to both the greater surface area of the rippled surface relative to a planar nickel surface and a thicker NiO_x layer generated by the laser process.

1. Introduction

Nickel is a widely used electrode material in battery technologies (*e.g.* nickel/cadmium, nickel/metal hydride, nickel/hydrogen, nickel/zinc, nickel/iron) [1]. Secondary battery technologies utilising a nickel cathode material and an alkaline electrolyte have nickel hydroxide, $Ni(OH)_2$ as the electrochemically active material. During charge/discharge electrode cycling, $Ni(OH)_2$ undergoes reversible oxidation to form the charged-state material, nickel oxyhydroxide, NiOOH. The ability of a nickel-based energy storage device to store and deliver power relies on the amount of the electrochemically active material that can accumulate at the electrode/electrolyte interface. It would be expected that maximising the accessible

* Corresponding authors.
E-mail addresses: s.p.edwardson@liverpool.ac.uk (S. Edwardson), laurence.hardwick@liv.ac.uk, laurence.hardwick@liverpool.ac.uk (L.J. Hardwick).

http://dx.doi.org/10.1016/j.jpowsour.2014.07.167

surface area of nickel cathodes would create a larger area for active material accumulation, leading to improved energy storage performance.

Efforts to improve the performance of nickel electrodes by maximising surface area have, so far, primarily involved the use of templating. Various techniques have been used to create templates onto which the electrode material can be deposited and, in some cases, the template can be subsequently removed, thus creating a nickel cathode framework. The template methods used so far include using; the micropores of an high internal phase emulsion polymer [2–4], the aqueous domains of a self-assembled liquid crystal template [5,6], the self-assembly of a mutant Tobacco mosaic virus to a gold surface [7,8] and a self-assembled opal template of 1.8 μm polystyrene spheres [9].

This work presents laser micro-structuring of nickel surfaces as an alternative to template-directed preparation. It has been shown previously that the surface of nickel metal, as well as other metals and semiconductors, can be rapidly modified with the use of ultrashort laser pulses [10–21]. The particular process of interest is the formation of laser-induced periodic plasmonic structures (LIPPS). These structures exist in the form of ripples at the solid surface and were first observed during the examination of semiconductor surface damage by a ruby laser [10].

It was initially proposed that the formation of LIPPS was a result of interference between the surface scattered wave and the incident laser radiation resulting in periodic spacings approximately equal to the laser wavelength [11,12]. This concept has been developed further based on the assumption that the formation of LIPPS occurs as a result of inhomogeneous energy deposition just beneath the surface [22,23]. Furthermore, some recent studies have also provided evidence to suggest that interference between the incident laser and exited surface plasmons may also contribute to the formation of LIPPS [13,15,19]. The ripples that result from the surface laser treatment form perpendicular to the direction of the lasers polarisation.

The formation of micro-structures at the nickel surface can be achieved extremely rapidly by laser-treatment (dependent on parameters and setup, typically 4 cm^2 per second is possible), removing the need for any complex or time-consuming synthesis steps required during templating. In particular, the treatment with ultrashort laser pulses to yield high surface area nickel electrodes could create materials for possible applications in micro-batteries. The nickel hydroxide/oxyhydroxide couple has been previously investigated as a possible micro-battery electrode in several different forms in addition to the previously described templating methods; thick-film printed electrodes using a mixture of nickel hydroxide, fine nickel metal powders and binder material as the ink [24], high-aspect ratio pillar nickel electrodes [25], hierachical micro-spheres and micro-flowers of $Ni(OH)_2$ [26] and graphene encapsulated nickel core–shell electrodes [27].

2. Experimental

2.1. Laser micro-structuring of nickel foils

High-purity nickel foils with a thickness of 1.0 μm (Goodfellow) were used in the preparation of the nickel electrodes. From a thin strip of nickel (ca. 25 × 8 mm) an area of 5 mm^2 was treated using ultra-short pulse length (femtosecond and picosecond) and low pulse energy (1–3 μJ per pulse) lasers. Two laser systems were used in this study; an amplified Ti:Sapphire laser (Clark-MXR CPA2010) and a custom made Nd:VAN seeded regenerative amplifier laser (High-Q IC-355-800 ps). The Clark-MXR laser system has a pulse length of 160 fs, a repetition rate of 1 kHz and a central wavelength of 775 nm, with a similar set-up to that detailed in Ref. [28]. The High-Q laser is a 10 ps pulse length laser system capable of repetition rates up to 50 kHz and output wavelengths of 1064 nm, 532 nm and 355 nm (355 nm wavelength pulses have not been used in this work). The overall set-up for the High-Q laser system is the same as detailed in Ref. [29]. Both set-ups used a scan head and f theta lens to deliver the laser beam to the work piece. All experiments described in this study used linearly polarised laser pulses. Samples were processed with the laser beam at a normal incident angle as the structure of LIPSS produced can be sensitive to this incident angle.

The laser spot was scanned across the planar nickel surface in parallel lines at a predefined scan rate (mm s^{-1}). The overall laser fluence (energy delivered per unit area) was controlled by varying parameters of the laser treatment; repetition rate, pulse intensity, diameter of the laser spot, the number of overlapping scans and the hatch distance (separation between the parallel scans).

2.2. Characterisation of nickel surfaces

The formation of the LIPPS at the nickel surface was characterised by scanning electron microscopy (SEM) and white-light interferometry. White-light interferometry measurements were completed on a WYKO NT1100 Optical Profiling System. SEM imaging was performed on a JEOL JSM-6610 instrument working at 30 keV.

2.3. Electrochemical analysis of laser-processed nickel

Electrochemical measurements were obtained using a standard three-electrode cell equipped with the nickel working electrode, a platinum wire counter electrode and a silver/silver chloride reference electrode. A 3 M KOH solution in distilled water was used as the electrolyte. All voltammetric measurements were conducted using a Bio-Logic VSP potentiostat at room temperature. To prepare the processed nickel foils for testing, the unprocessed nickel surface was coated in a few layers of insulating acrylic lacquer to create an exposed, well-defined geometric area of purely laser-processed nickel metal. A platinum wire was attached to the nickel using silver conducting paste to ensure a good electrical contact. The nickel strip was washed in a small amount of additional 3 M KOH electrolyte solution prior to immersion into the electrolyte.

Cyclic voltammetry of the different nickel samples was performed in a potential range of 0–0.45 V vs. Ag/AgCl to study the oxidation/reduction peaks of the $Ni(OH)_2$/NiOOH couple. The nickel was cycled at a range of scan rates from 10 mV s^{-1} to 2500 mV s^{-1}. These measurements were compared with control samples of unprocessed nickel metal foil.

2.4. Surface characterisation of the laser processed nickel

Raman spectra were recorded with a Raman microscope (Renishaw inVia), using a 633 nm wavelength laser focussed through an upright microscope (Leica), via a 50× objective (Leica). X-ray photoelectron (XPS) experiments were performed in a standard ultrahigh vacuum surface science chamber consisting of a PSP Vacuum Technology electron energy analyser (angle integrating ± 10°) and a dual anode X-ray source. [30] The base pressure of the system was less than 2×10^{-10} mbar, with hydrogen as the main residual gas in the chamber. The XPS measurements were carried out with a Mg K-alpha source (1253.6 eV). The spectrometer was calibrated using Au $4f_{7/2}$ at 83.9 eV. The samples were corrected for charging using the adventitious carbon 1s peak.

3. Results and discussion

3.1. Formation of LIPPS

At a macroscopic level the laser-processed area of the nickel strip was observed to reflect natural light differently compared to the planar unprocessed area, making it apparent which section of the metal had been Laser treated. Initial analysis using white-light interferometry (Fig. 1) of processed nickel foils showed the consistent formation of LIPPS as a result of laser treatment at 775 nm and 1064 nm. The direction in which the rippled structures formed was perpendicular to the polarisation of the light. This is consistent with the experimental results described in previous literature [28,31]. The coverage of the LIPPS at the nickel surface is determined by both the laser spot radius and the hatch distance. If the hatch distance (the spacing between parallel laser scans) is less than the laser spot radius, the processed area of the scans will partially overlap, giving a greater coverage of treated nickel. Fig. 1(c) shows a sample prepared using a laser spot radius of 15 μm and a 10 μm hatch spacing to give what appears as 100% coverage of LIPPS. Fig. 1(b) shows a sample prepared using a 20 μm spacing (*i.e.* greater than the laser spot radius) indicating rippled (yellow arrow) and planar (red arrow) (in web version) lines across the surface. This sample, therefore, has LIPPS coverage of less than 100%.

The four SEM images (Fig. 2(a)–(d)) demonstrate the long-range periodicity of the LIPPS generated at the nickel surfaces. The samples imaged in Fig. 2 were generated using the 1064 nm laser and the periodicity of the ripple structures, ≈1 μm, is approximately equal to the laser wavelength used. This is consistent with observations reported previously [21,23,31]. Topographical information derived from the white-light interferometry analysis (Fig. 1(d)) shows that in the samples generated using the 775 nm wavelength laser, the periodicity of the ripples was also approximately equal to the laser wavelength. Structures in which the periodic spacings are approximately equal to the laser wavelength, like those produced in this work, are known as Low Spatial Frequency LIPPS (LSFL) [31]. Sub-wavelength periodicity structures, referred to as High Spatial Frequency LIPPS (HSFL), have also been reported for nickel [13,14] and other materials [15–20].

Fig. 2(d) shows a boundary edge of the laser-processing, highlighting the difference between the LIPPS and the planar surface of the nickel. The image demonstrates the ripples at the boundary are much less pronounced than those in the bulk of the LIPPS. This can be attributed to the Gaussian energy distribution of the laser spot. The laser fluence at the boundary of the laser spot is lower compared to the center of the spot, where the greatest laser intensity is distributed. Consequently, a decreasing gradient of energy is delivered to the surface towards the boundary of the laser spot

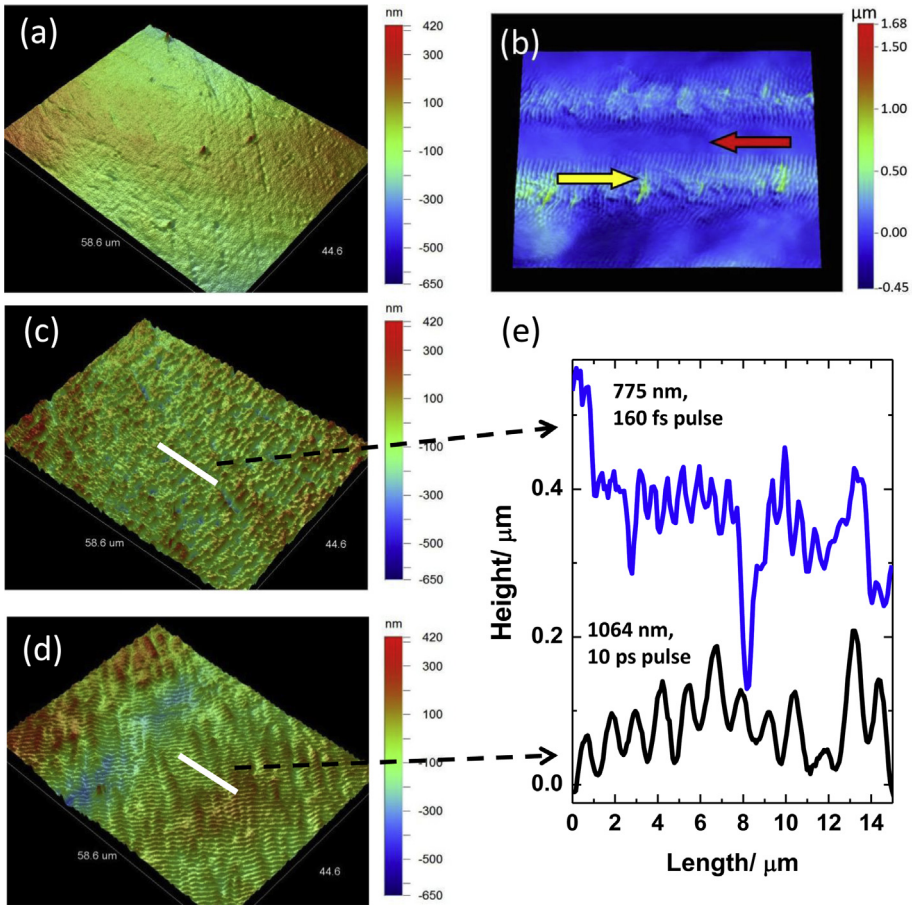

Fig. 1. White-light interferometry of nickel surfaces; (a) image of an unprocessed, planar nickel surface; (b) image of partial LIPPS coverage as a result of no overlapping laser scans (1064 nm laser) (c) complete LIPPS coverage across the entire nickel surface; (775 nm laser). (d) complete LIPPS coverage across the entire nickel surface; (1064 nm laser) (e) depth and periodicity profile of LIPPS, of white line trace shown in (c) and (d).

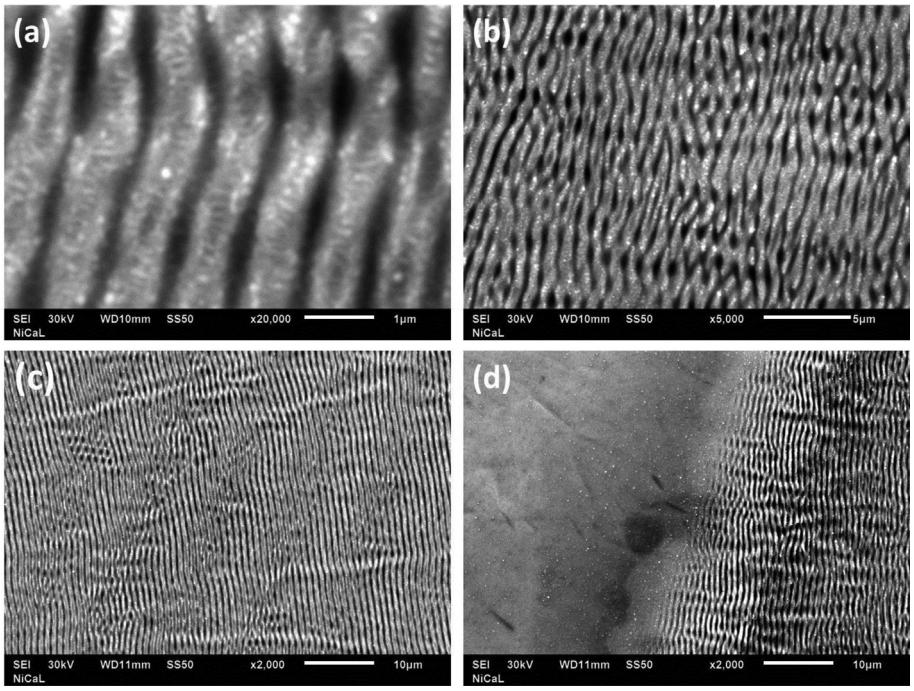

Fig. 2. Scanning electron micrographs of LIPPS on nickel surfaces. Imaged samples were processed using a 1064 nm wavelength picosecond laser: Images (a–c) show the LIPPS formations across the full range of the image, (d) shows the boundary of laser-processing, showing a relatively planar unprocessed nickel surface and the LIPPS ripples.

and this results in the production of a decreasing gradient in the depth of ripples towards the boundary.

3.2. Electrochemical performance

The cyclic voltammogram of a laser-processed nickel foil and an untreated nickel foil is shown in Fig. 3. The anodic and cathodic peaks observed between 0.2 and 0.4 V vs. Ag/AgCl, attributed to the oxidation and subsequent reduction of a few monolayers of surface

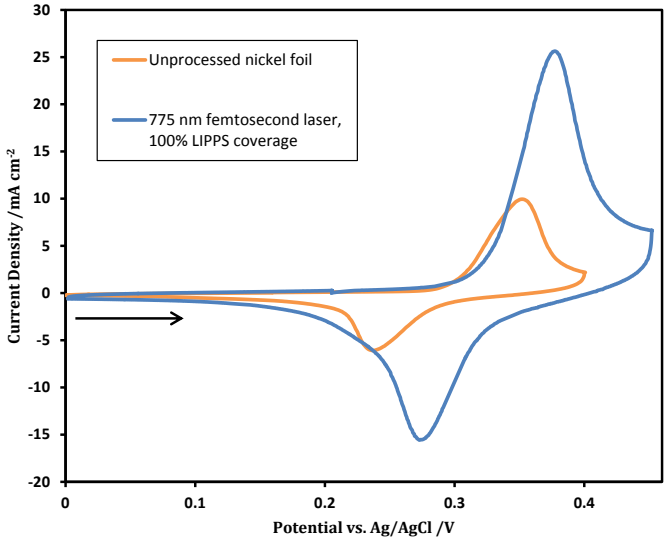

Fig. 3. Cyclic voltammetry at 500 mV s^{-1} of a LIPPS nickel electrode and an unprocessed nickel foil electrode. Laser parameters used to generate LIPPS: Clark-MXR femtosecond laser, 775 nm central wavelength, 1.5 μJ $pulse^{-1}$, 1 kHz, 178 mm s^{-1} laser scan rate, 17 overlaps on one spot area.

$Ni(OH)_2$ (Eq. (1)), are consistent typical of those reported in the literature [5,32,33].

$$Ni(OH)_2 + OH^- \rightleftharpoons NiOOH + H_2O + e^- \quad (1)$$

To compare the electrochemical activity of the nickel cathodes, the anodic peak current densities associated with the formation of NiOOH were compared at equivalent scan rates. From Fig. 3, it can be seen that the anodic peak current for this particular laser-processed sample (25.6 mA cm^{-2}) was over 2.5 times greater than the equivalent peak current density for the unprocessed nickel electrode (9.9 mA cm^{-2}), with associated charges of ca. 1.2 mC cm^{-2} for the unprocessed nickel foil and 4 mC cm^{-2} for the processed sample. A change of potential difference between the anodic and cathodic peaks can also be observed with the unprocessed foil having a wider difference of 0.11 V compared to 0.09 V for the laser processed Ni foil. This may result from different surface properties of the films, which will discussed be later on.

Fig. 4 shows the measured anodic peak current densities across the full range of scan rates. The best enhancement in electrochemical activity was observed when the sample was prepared with 100% LIPPS coverage and with the 775 nm wavelength laser. Utilising the understanding that the presence of LIPPS at the surface yields an increased surface area, it is clear that achieving the maximum (100%) LIPPS coverage is expected to have the greatest effect on the activity. This expectation is confirmed by comparing the two samples prepared with the 775 nm wavelength laser (and with a laser spot radius of 15 μm); the sample with less than 100% coverage was prepared with a 20 μm hatch spacing and shows considerably less enhancement than the equivalent sample prepared with a 10 μm hatch spacing (100% LIPPS coverage).

Two main features of the ripple micro-structures would be expected to contribute to the overall change in surface area as a result of LIPPS formation; the periodic spacing of the ripples and the amplitude of the ripples. It was observed during experimentation that more pronounced ripples were produced when longer

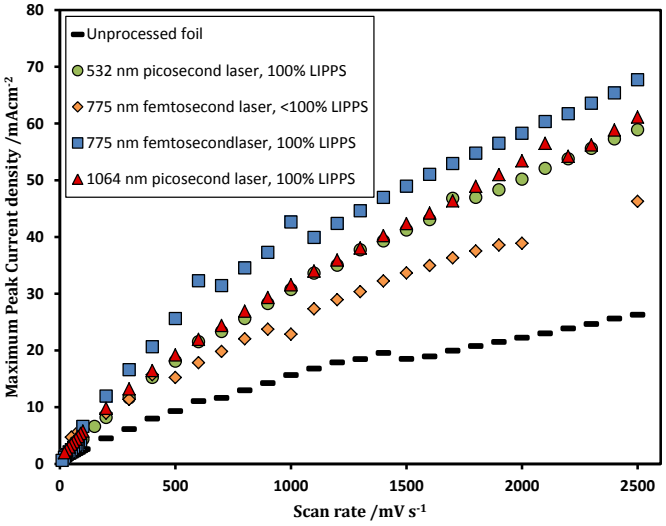

Fig. 4. Anodic peak current density values for full range of scan rates. % LIPPS corresponds to LIPPS coverage across the nickel surface.

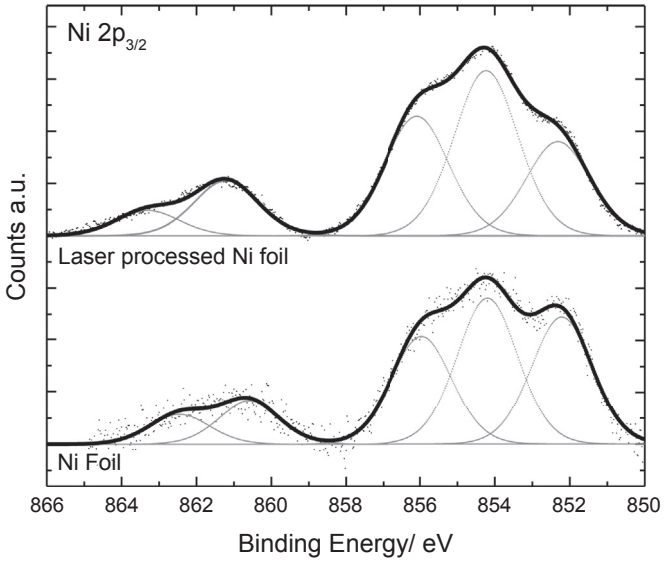

Fig. 6. X-ray photoelectron spectra records for the unprocessed nickel foil and laser processed nickel foil (775 nm, 160 fs pulse).

wavelength laser radiation was used to create the LIPPS (Fig. 1(c,d)). However, as stated previously, since the periodicity of the ripples approximately equals the wavelength of the laser, smaller wavelength pulses are observed to produce smaller periodic spacings, as observed from the line scans obtained from white-light interferometry (Fig. 1(e)) from 775 to 1064 nm wavelength processed Ni substrates. By considering the balance between these two contributing factors, it is possible to understand why the middle wavelength radiation, 775 nm, yielded the greatest overall enhancement. Using the 775 nm wavelength laser produced a rippled nickel surface with more distinct peaks and troughs than the 532 nm sample and shorter periodic spacings than the 1064 nm sample (Fig. 1(c–e)). This resulted in a greater surface area than the two corresponding samples. However, it is unclear whether surface area effects alone as a result of LIPPS formation are solely responsible in the observed enhancement in current density. Raman and X-ray photoelectron spectroscopy was used to characterise the nature of the NiO_x on the surface of Ni metal on the unprocessed and laser processed Ni foil.

Fig. 5 shows the Raman spectra collected from the as received Ni foils and a Ni foil treated by the775 nm laser. The Ni foil displayed a weak band at ca. 537 cm^{-1} that can be assigned to the Ni—O stretching mode and this is typical signal for the NiO_x layer on Ni metal surfaces [34,35]. For the laser treated sample a much stronger and sharper peak is observed suggesting a greater presence of NiO_x on the surface from both the higher surface area and from a thicker layer of NiO_x. The thicker layer was confirmed by XPS measurements (Fig. 6), where the ratio of metallic Ni to NiO_x is higher in the untreated foil, as seen by the relatively larger intensity peak of metallic Ni at 852.2 eV, compared to the other four peaks assigned to NiO. The line shape of the Ni 2p was compared to that in the literature and agrees with the features for NiO_x [36], suggesting that apart from a thicker NiO_x layer, the chemical nature of both foils at the surface are identical. It is believed that the thicker NiO_x layer is generated by the short heat pulse from the laser during LIPPS formation; whereby localized surface heating generates a thicker

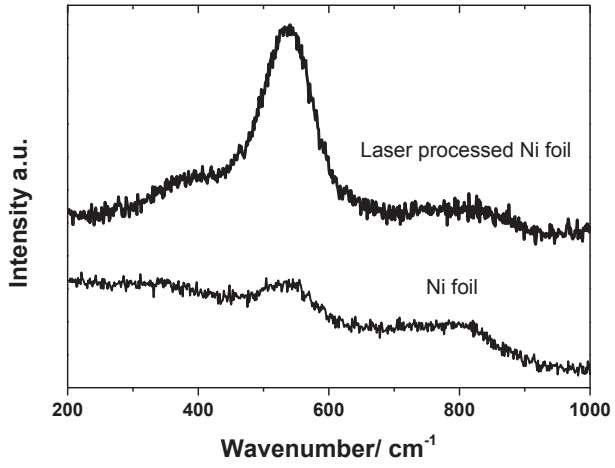

Fig. 5. Raman spectra of an unprocessed nickel foil and laser processed nickel foil (775 nm, 160 fs pulse).

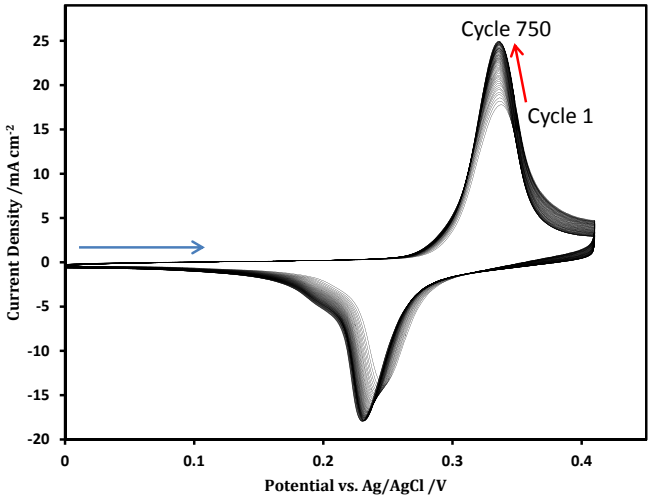

Fig. 7. Cyclic voltammograms of sample "532 nm ps laser, 100% LIPPS". The potential of the working electrode was cycled 750 times at a constant scan rate of 500 mV s^{-1}.

oxide layer and accounts for the differences in the position and separation of the anodic and cathodic peaks during CV scans.

Finally, to assess the stability of the LIPPS nickel, the electrodes were cycled continuously for 750 cycles. Fig. 7 shows the current peaks for both the anodic and cathodic reactions remain relatively stable for the period of extended cycling. The current density peaks increase slightly with cycle number. This effect could be attributed to the further thickening of the electrochemically active layer at the nickel electrode/electrolyte interface.

4. Conclusion

The surface of nickel metal foils was processed with the use of ultra-short pulse length, low energy laser light. This rapid technique (4 cm^2 per second, with higher possible) was shown to produce periodic ripple micro-structures (LIPPS) on the surface of the nickel metal. Cyclic voltammetry was used to demonstrate that the formation of the ripples yields increased electrochemical activity relative to unprocessed planar nickel by 2.5 times. The observed improvement is attributed to both the increase in surface area as a result of ripple formation and the thickening of the NiO_x overlayer on nickel by localised surface heating during the laser process, as evidenced from Raman spectroscopy and XPS data. The use of laser-processing techniques to modify the electrode surface at the micro-scale is a very rapid technique, eliminating any complex or time-consuming synthetic steps, thus creating an additional option for producing high surface area electrodes for nickel-based micro-battery systems.

Further optimisation of the laser-processing technique should involve maximising the overall surface area enhancement by producing deeper troughs with smaller periodic spacings between the ripple structures. Creating a more uniform formation of the ripples across the entire surface area is also desirable, this could be achieved by controlling the intensity distribution of the laser spot dynamically, *i.e.* using a top-hat beam shape with a more uniform intensity distribution [37]. This method, if implemented, could be used to give a more uniform distribution of the laser fluence at the nickel surface and result in a more uniform formation of the ripple structures.

Acknowledgements

Support from the EPSRC Shaping Capability Institutional Fund and the EPSRC Great Technologies: Grid-scale Energy Storage grant (EP/J021229/1) and the Nanoinvestigation Centre at Liverpool (NiCaL) are gratefully acknowledged.

References

[1] D. Linden, T.B. Reddy, Handbook of Batteries, third ed., McGraw-Hill, 2002.
[2] I. Brown, S. Sotiropoulos, J. Appl. Electrochem. 30 (2000) 107–111.
[3] I.J. Brown, D. Clift, S. Sotiropoulos, Mater. Res. Bull. 34 (1999) 1055–1064.
[4] I.J. Brown, S. Sotiropoulos, Electrochim. Acta 46 (2001) 2711–2720.
[5] P.A. Nelson, J.M. Elliott, G.S. Attard, J.R. Owen, Chem. Mater. 14 (2002) 524–529.
[6] P.A. Nelson, J.M. Elliott, G.S. Attard, J.R. Owen, J. New. Mat. Elec. Syst. 5 (2002) 63–65.
[7] K. Gerasopoulos, M. McCarthy, E. Royston, J.N. Culver, R. Ghodssi, J. Micromech. Microeng. 18 (2008) 104003.
[8] E. Royston, A. Ghosh, P. Kofinas, M.T. Harris, J.N. Culver, Langmuir 24 (2008) 906–912.
[9] H. Zhang, X. Yu, P.V. Braun, Nat. Nanotechnol. 6 (2011) 277–282.
[10] M. Birnbaum, J. Appl. Phys. 36 (1965) 3688–3689.
[11] M. Oron, G. Sorensen, Appl. Phys. Lett. 35 (1979) 782–784.
[12] D.C. Emmony, R.P. Howson, L.J. Willis, Appl. Phys. Lett. 23 (1973) 598–600.
[13] F. Garrelie, J.P. Colombier, F. Pigeon, S. Tonchev, N. Faure, M. Bounhalli, S. Reynaud, O. Parriaux, Opt. Express 19 (2011) 9035–9043.
[14] J.-W. Yao, C.-Y. Zhang, H.-Y. Liu, Q.-F. Dai, L.-J. Wu, S. Lan, A.V. Gopal, V.A. Trofimov, T.M. Lysak, Opt. Express 20 (2012) 905–911.
[15] J. Bonse, A. Rosenfeld, J. Krüger, in: International Conference on Lasers, Applications, and Technologies, 2010, p. 79940M.
[16] E. Freysz, S.M. Pershin, G.A. Shafeev, in: Proceedings of the Society of Photo-optical Instrumentation Engineers, vol. 5850, 2005, pp. 82–87.
[17] M. Huang, F. Zhao, Y. Cheng, N. Xu, Z. Xu, ACS Nano 3 (2009) 4062–4070.
[18] L.L. Ran, S.L. Qu, Appl. Surf. Sci. 256 (2010) 2315–2318.
[19] J.C. Wang, C.L. Guo, J. Appl. Phys. 100 (2006) 023511.
[20] Y. Yang, J.J. Yang, C.Y. Liang, H.S. Wang, X.N. Zhu, D.F. Kuang, Y. Yang, Appl. Phys. A-mater. Sci. Process. 92 (2008) 635–642.
[21] A. Borowiec, H.K. Haugen, Appl. Phys. Lett. 82 (2003) 4462–4464.
[22] J.E. Sipe, J.F. Young, J.S. Preston, H.M. van Driel, Phys. Rev. B 27 (1983) 1141–1154.
[23] J.F. Young, J.S. Preston, H.M. Vandriel, J.E. Sipe, Phys. Rev. B 27 (1983) 1155–1172.
[24] W.G. Tam, J.S. Wainright, J. Power Sources 165 (2007) 481–488.
[25] F. Chamran, H.S. Min, B. Dunn, C.J. Kim, IEEE, in: MEMS 2006: 19th IEEE International Conference on Micro Electro Mechanical Systems, Technical Digest, IEEE, New York, 2006, pp. 950–953.
[26] Y. Wang, Q. Zhu, Mater. Res. Bull. 45 (2010) 1844–1849.
[27] X. Xiao, J.R. Michael, T. Beechem, A. McDonald, M. Rodriguez, M.T. Brumbach, T.N. Lambert, C.M. Washburn, J. Wang, S.M. Brozik, D.R. Wheeler, D.B. Burckel, R. Polsky, J. Mater. Chem. 22 (2012) 23749–23754.
[28] O.J. Allegre, W. Perrie, S.P. Edwardson, G. Dearden, K.G. Watkins, J. Opt. 14 (2012) 085601.
[29] Z. Kuang, W. Perrie, D. Liu, P. Fitzsimons, S.P. Edwardson, E. Fearon, G. Dearden, K.G. Watkins, Appl. Surf. Sci. 258 (2012) 7601–7606.
[30] K.H.L. Zhang, I.M. McLeod, M. Lahti, K. Pussi, V.R. Dhanak, J. Phys.-Condens. Matter 24 (2012) 435502.
[31] J.Z.P. Skolski, G. Romer, J.V. Obona, V. Ocelik, A.J.H. in 't Veld, J.T.M. De Hosson, Phys. Rev. B 85 (2012).
[32] M. Amjad, D. Pletcher, C. Smith, J. Electrochem. Soc. 124 (1977) 203–206.
[33] L.D. Burke, T.A.M. Twomey, J. Electroanal. Chem. 162 (1984) 101–119.
[34] S.H. Lee, H.M. Cheong, N.G. Park, C.E. Tracy, A. Mascarenhas, D.K. Benson, S.K. Deb, Solid State Ionics 140 (2001) 135–139.
[35] K.W. Nam, K.B. Kim, J. Electrochem. Soc. 149 (2002) A346–A354.
[36] H.W. Nesbitt, D. Legrand, G.M. Bancroft, Phys. Chem. Minerals 27 (2000) 357–366.
[37] B. Tan, K. Venkatakrishnan, J. Micromech. Microeng. 16 (2006) 1080–1085.